Effect of electron-beam momentum spread on cyclotron resonance maser operation at two resonant frequencies

G. J. Hunter,* B. W. J. McNeil, and G. R. M. Robb
Department of Physics and Applied Physics, University of Strathclyde, Glasgow, G4 0NG, Scotland
(Received 5 February 2001; published 28 August 2001)

We present a theoretical analysis of cyclotron resonance maser (CRM) operation at two resonant frequencies including the effects of momentum spread in the electron beam. A linear analysis of the system equations is presented in the limit of small momentum spreads. Numerical solutions to the system equations are also given and are in agreement with the linear theory. The results predict that for realistic momentum spreads, operation of the CRM at the higher of the two resonant frequencies should be possible, extending its operating frequency range. An experiment currently under development at Strathclyde University is described and modeled numerically.

DOI: 10.1103/PhysRevE.64.036502 PACS number(s): 41.60.−m, 52.59.Px, 84.40.Ik

I. INTRODUCTION

Cyclotron resonance masers (CRMs) are important sources of coherent high power microwave radiation [1]. The radiation source of the CRM is a relativistic electron beam gyrating as it propagates along a uniform magnetic field. The radiation emitted is usually contained within a cylindrical waveguide structure. When the electrons interact with either their spontaneous radiation, or with an injected signal, a collective instability may bunch the electrons in the phase angle of the electron gyration, or the axial electron position, or both. The bunched electrons may then emit coherently. The collective instability may give an exponential growth of the radiation field until saturation, where free energy depletion of the electron beam [2,3] and/or a dephasing of the electron bunching occurs. In general, for a single waveguide mode, there exist two distinct resonant frequencies. In most circumstances it is the lower resonant frequency that has the larger growth rate and dominates the exchange of energy from the electrons to the radiation field [4]. However, in an analysis of the steady state amplifier interaction, which assumes a uniform current electron beam source of infinite duration, it was shown that allowing both the lower and higher resonant frequency fields to evolve, it is possible to suppress the evolution of the lower frequency instability [4]. This may allow the CRM to operate at the higher frequency only. When the CRM has electron pulses as its source, and consequently the steady state approximation is not valid, the relative propagation of the electron pulse with respect to the radiation emitted becomes important and gives rise to new regimes of operation [5]. These regimes include super radiance, where the radiation intensity scales as the square of the pulse current, and ''pulse suppression'' of the lower resonant frequency. In this paper we assume a steady state interaction and investigate the effects of an electron beam momentum spread on the operation of the two frequency CRM. This is of importance to any experimental program of work designed to observe operation at the higher frequency. A set of equations is derived which includes the effects of momentum spread on the electron-radiation interaction. These equations are the subject of a linear analysis which yields a logarithmic dispersion relation. This relation is used to explore the regions of parameter space where exponential growth of the lower and higher frequencies occurs. Full numerical solutions of the electron-radiation evolution equations extend the analysis into the nonlinear regime enabling saturation effects and nonlinear coupling between the lower and higher frequencies to be investigated. Finally we give details and simulations of an experimental program being developed at Strathclyde University to investigate two frequency operation of CRMs.

II. THE MODEL

The notation used in our model of the CRM interaction is the same as that used in previous publications [4,5] to which reference can be made for further details. The resonant frequencies of the CRM interaction may be determined by the intersection of the waveguide and beam modes as defined by $\omega^2=\omega_c^2+k_\parallel^2c^2$ and $\omega=\omega_H+k_\parallel v_\parallel$, respectively, where ω_c is the waveguide cutoff frequency, $k_\parallel$ is the axial component of the radiation wave vector, ω_H is the relativistic cyclotron frequency and $v_\parallel$ is the axial velocity of the electrons. A typical dispersion diagram shows intersections at two resonant frequencies in Fig. 1. The radiation at the higher resonant frequency has an axial group velocity ($v_g=\partial\omega/\partial k_\parallel$) greater than that of the lower resonant frequency and so we call these resonant modes the ''fast'' and ''slow'' resonant modes, respectively. Solving the equations of the beam and waveguide modes we obtain expressions for the fast and slow mode resonant frequencies and their corresponding axial wave vectors

$$\omega_{f,s}=\omega_H\frac{1\pm\beta_\parallel\sqrt{1-X}}{1-\beta_\parallel^2} \tag{1}$$

and

$$k_{\parallel f,s}=\frac{\omega_H}{c}\frac{\beta_\parallel\pm\sqrt{1-X}}{1-\beta_\parallel^2}, \tag{2}$$

where the ''waveguide parameter'' $X=\omega_c^2/(\omega_H^2\gamma_\parallel^2)$, $\beta_\parallel=v_\parallel/c$, $\gamma_\parallel=(1-\beta_\parallel^2)^{-1/2}$ and subscripts ''f'' and ''s'' indi-

*Email address: gordon.hunter@strath.ac.uk

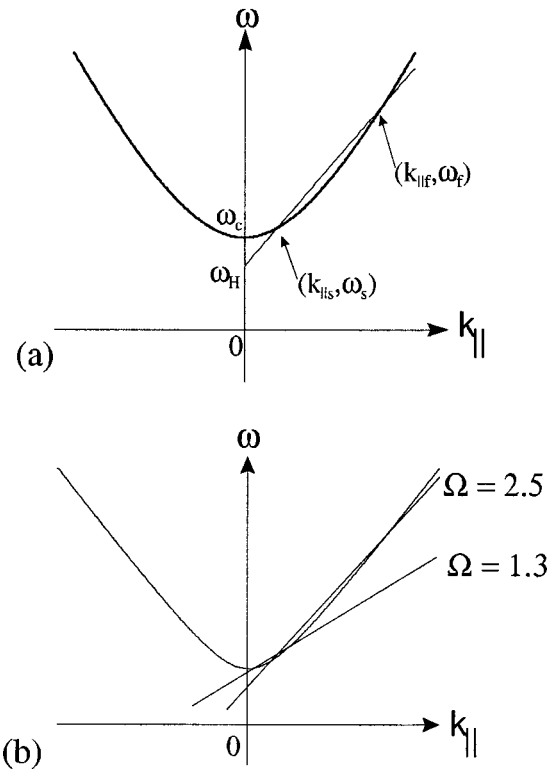

FIG. 1. (a) Dispersion diagram showing the intersection of electron beam and waveguide modes. (b) Dispersion diagram illustrating the different operating regimes for two values of the device parameter Ω for $\epsilon=2$ ($\Omega_{max}=4$).

cate the fast and slow modes, respectively. The waveguide parameter must lie within the range $4\epsilon^3/(\epsilon^3+1)^2<X<1$ where $\epsilon^3=k_{\|f}/k_{\|s}$ [5].

The ''device parameter'' Ω, is defined as $\Omega=2/X-1=(\omega_f\omega_s-k_{\|f}k_{\|s}c^2)/\omega_c^2$ [5], and is constrained to lie within the limits $1<\Omega<(1+\epsilon^6)/(2\epsilon^3)$.

If Ω lies towards the minimum of the interval then the interaction is of the gyrotron type, conversely if Ω lies towards the maximum of the interval then the interaction is of the cyclotron autoresonance maser type.

Two other physically meaningful scaling parameters, defined below, are the fundamental CRM parameter ρ, analogous to the Pierce parameter of the traveling wave tube (TWT) theory [6] and determining the growth rate of the electron-radiation instability, and the depletion parameter μ, which describes the effects of free energy depletion of the electron beam [2,3]. The depletion parameter is a measure of the ability of the interaction to convert the energy associated with the cyclotron motion of the electrons into radiation. For small values of the depletion parameter only a small fraction of this transverse energy is available. Furthermore, in a single frequency interaction, linear theory shows that there is a threshold value of $\mu=\mu_{\rm th}$, above which there can be no exponential growth of the radiation field [3].

In a two frequency interaction we are free to choose the principle scaling parameters from the ρ and μ parameters of the fast or the slow modes [5]. In this paper the fast mode scaling is chosen, conversion to slow mode scaling being straightforward via the relations: $\rho_f=\epsilon^2\rho_s$ and $\mu_f=\mu_s/\epsilon$. Note that ρ_f is bounded within the interval $0<\rho_f<2\mu_f\epsilon^3/(\epsilon^3+1)$. The upper limit of ρ_f restricts the maximum growth rate of the radiation and also the efficiency of the device [4].

A linear and numerical analysis of the coupled two frequency mode interaction has been conducted in the steady state regime when electron momentum spread effects are neglected [4] (so that initial conditions for electron momenta are identical). Here, the slow mode has a larger growth rate, except for a small region of parameter space where linear theory and numerical simulation predict no exponential growth of the slow mode for a range of the depletion parameter μ_f. This range corresponds to that where, due to the relation $\mu_f=\mu_s/\epsilon$, the value of the depletion parameter of the fast mode is below threshold ($\mu_f<\mu_{\rm th}$), but that for the slow mode is above threshold ($\mu_s>\mu_{\rm th}$). Hence, choice of μ_f from within this region allows for a ''μ suppression'' of the lower frequency slow mode.

Summarizing, in total four parameters are required to describe the CRM coupled interaction between the fast and slow modes: the axial wave vector ratio ϵ^3; the device parameter Ω; the CRM parameter for the fast mode ρ_f; and the depletion parameter of the fast mode μ_f.

This paper investigates the effects of an initial momentum spread in the electron beam on the two frequency operation of a CRM. The model developed is then used to predict the characteristics of an experiment designed to investigate two frequency CRM operation currently under development at Strathclyde University. It may be expected that a spread in electron beam momentum would have a greater detrimental effect on higher frequency radiation amplification than on that of the lower frequency. The degree of spatial (axial) bunching and phase bunching required of the electrons is greater at higher radiation frequencies, and so the amount of dephasing, due to a given electron momentum spread, will be greater at the higher frequency. We use an analytical and numerical analysis to show that, while this is true, it should still be possible to achieve CRM operation at the higher of the two resonant frequencies.

The equations describing the two frequency CRM interaction were derived from the coupled Maxwell–Lorentz equations which describe the radiation and electron beam evolution [3]. A thin annular electron beam co-propagating in the positive $\hat{\mathbf{z}}$ direction along a cylindrical waveguide containing ''cold'' $\mathrm{TE}_{m,n}$ waveguide modes is assumed. The waveguide is coaxial with a static magnetic field $\mathbf{B}=B_0\hat{\mathbf{z}}$. These modes are defined by the cylindrical components of the electric fields

$$E_{f,s}^{(r)}=-\frac{m}{2r}F_{f,s}(z,t)D_{TE}J_m(k_\perp r)e^{i\Psi_{f,s}}+\text{c.c.}$$

$$E_{f,s}^{(\theta)}=\frac{ik_\perp}{2}F_{f,s}(z,t)D_{TE}J_m'(k_\perp r)e^{i\Psi_{f,s}}+\text{c.c.}$$

$$E_{f,s}^{(z)}=0,$$

where

$$\Psi_{f,s}=\omega_{f,s}t-m\theta-k_{\|f,s}z, \quad D_{TE}=\frac{1}{J_m(\chi'_{mn})\sqrt{\pi(\chi'^2_{mn}-m^2)}},$$

$k_\perp$ is the transverse component of the radiation wave vector, χ'_{mn} is the nth root of $J'_m(k_\perp R_w)=0$, and R_w is the waveguide radius. The field is assumed to obey the slowly varying envelope approximation (SVEA) so that $F_{f,s}(z,t)=|F_{f,s}(z,t)|e^{i\xi_{f,s}(z,t)}$ is a slowly varying complex envelope function determining the z and t dependence of the amplitude and phase of the radiation field.

The product of the transverse component of the radiation wave vector and the Larmor radius of the gyrating electrons is assumed small, i.e., $k_\perp r_L<1$. Experimentally, this allows the electron beam annulus to be coincident with the maximum of the transverse mode electric field, maximizing the coupling between electron beam and the radiation mode. Further, it is assumed there are no space charge effects and the electron beam phase evolution is slow with respect to the cyclotron period. The latter allows the Maxwell–Lorentz equations to be averaged over a cyclotron period. The effect of beating between the two radiation frequencies is also neglected by averaging the wave equations over a beat period, which under SVEA is valid for $\omega_f \gtrsim 2\omega_s$. Further details of the one and two frequency theory, including the derivation of the evolution equations, can be found in Refs. [3–5]. With these approximations the coupled Maxwell–Lorentz equations reduce to

$$\frac{d\phi_{f_j}}{d\bar{z}_f}=\bar{p}_{f_j}-\frac{i\mu_f}{\bar{u}_{\perp_j}\bar{u}_{\|_j}}(\bar{A}_f e^{i\phi_{f_j}}+\epsilon^2\bar{A}_s e^{i\phi_{s_j}}-\text{c.c.}), \tag{3}$$

$$\frac{d\phi_{s_j}}{d\bar{z}_f}=\epsilon\bar{p}_{s_j}-\frac{i\mu_f}{\bar{u}_{\perp_j}\bar{u}_{\|_j}}(\bar{A}_f e^{i\phi_{f_j}}+\epsilon^2\bar{A}_s e^{i\phi_{s_j}}-\text{c.c.}), \tag{4}$$

$$\frac{d\bar{p}_{f_j}}{d\bar{z}_f}=\frac{\bar{u}_{\perp_j}}{\bar{u}^2_{\|_j}}\left[(\rho_f\bar{p}_{f_j}-1)\bar{A}_f e^{i\phi_{f_j}}+\left(\frac{\rho_f}{\epsilon}\bar{p}_{f_j}-\epsilon^2\Omega\right)\bar{A}_s e^{i\phi_{s_j}}+\text{c.c.}\right], \tag{5}$$

$$\frac{d\bar{p}_{s_j}}{d\bar{z}_f}=\frac{\bar{u}_{\perp_j}}{\bar{u}^2_{\|_j}}\left[\left(\rho_f\bar{p}_{s_j}-\frac{\Omega}{\epsilon}\right)\bar{A}_f e^{i\phi_{f_j}}+\left(\frac{\rho_f}{\epsilon}\bar{p}_{s_j}-\epsilon\right)\bar{A}_s e^{i\phi_{s_j}}+\text{c.c.}\right], \tag{6}$$

$$\frac{d\bar{u}_{\perp_j}}{d\bar{z}_f}=-\frac{\mu_f}{\bar{u}_{\|_j}}(\bar{A}_f e^{i\phi_{f_j}}+\epsilon^2\bar{A}_s e^{i\phi_{s_j}}+\text{c.c.}), \tag{7}$$

$$\frac{d\bar{u}_{\|_j}}{d\bar{z}_f}=-\frac{\bar{u}_{\perp_j}\rho_f}{\bar{u}_{\|_j}}\left(\bar{A}_f e^{i\phi_{f_j}}+\frac{1}{\epsilon}\bar{A}_s e^{i\phi_{s_j}}+\text{c.c.}\right), \tag{8}$$

$$\frac{d\bar{A}_f}{d\bar{z}_f}=\bar{b}_f, \tag{9}$$

$$\frac{d\bar{A}_s}{d\bar{z}_f}=\epsilon\bar{b}_s, \tag{10}$$

where

$$j=1,\ldots,N, \quad \bar{z}_f=\frac{z}{l_{g_f}},$$

$$\phi_{f,s}=\omega_{f,s}t-k_{\|f,s}z+\tan^{-1}\left(\frac{u_y}{u_x}\right)-(m-1)\theta_0-\frac{\pi}{2},$$

$$\bar{u}_\perp=\frac{u_\perp}{\langle u_{\perp 0}\rangle}, \quad \bar{u}_\|=\frac{u_\|}{\langle u_{\|0}\rangle}, \quad u_\perp=\gamma v_\perp, \quad u_\|=\gamma v_\|,$$

$$\bar{A}_{f,s}=\frac{ie\langle u_{\perp 0}\rangle k^2_{\|f,s}D_{TE}J_{m-1}(k_\perp R_0)}{4m_e\langle u_{\|0}\rangle^2 k_\perp\omega_{f,s}\rho^2_{f,s}}F_{f,s},$$

$$\bar{p}_{f,s}=\frac{k_{\|f,s}}{k^2_\perp}\frac{1}{\rho_{f,s}}p_{f,s}, \quad p_{f,s}=\frac{1}{v_\|}(\omega_{f,s}-\omega_H)-k_{\|f,s},$$

$$k_{H0}=\frac{\gamma\omega_H}{\langle u_{\|0}\rangle},$$

$$\rho_{f,s}=\left(\frac{e}{8\epsilon_0 m_e c^2}\frac{k^2_{\|f,s}}{k^2_\perp}\frac{\langle u_{\perp 0}\rangle^2}{\langle u_{\|0}\rangle^3}ID^2_{TE}J^2_{m-1}(k_\perp R_0)\right)^{1/3},$$

$$\nu_{f,s}=\frac{k_{\|f,s}}{k_{H0}}\frac{\langle u_{\perp 0}\rangle^2}{\langle u_{\|0}\rangle^2}, \quad \mu_{f,s}=\frac{\rho_{f,s}}{\nu_{f,s}}, \quad l_{g_f}=\frac{k_{\|f}}{k^2_\perp\rho_f},$$

$$\bar{b}_{f,s}=\left\langle\frac{\bar{u}_\perp}{\bar{u}_\|}e^{-i\phi_{f,s}}\right\rangle \text{ and}$$

$$\langle\cdots\rangle=\frac{1}{N}\sum_{j=1}^{N}(\cdots)$$

and j is the electron index number, N is the total number of electrons in a beat period, subscripts $\perp$ and $\|$ represent vector components perpendicular and parallel to the waveguide axis, r_L is the Larmor radius of a gyrating electron, γ is the electron relativistic factor, (R_0,θ_0) are the polar coordinates with respect to the waveguide axis of the electron guiding centers, $(v_\perp, v_\|)$ are the electron momentum components, l_{g_f} is the gain length for the fast mode in absence of electron momentum spread [4] and subscripts 0 indicate initial values on entering the interaction region at $\bar{z}_f=0$. The geometry of the electron beamlet illustrating the geometric variables is shown in Fig. 2. We assume that there is no cavity feedback so that the system acts as a single pass amplifier.

Note that in the continuous limit the average over the beat period may be written as

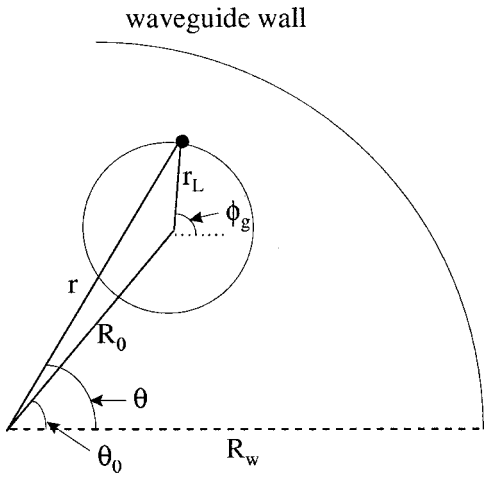

FIG. 2. A schematic of an electron beamlet showing the relevant geometry.

$$\langle\cdots\rangle=\frac{1}{n_{f,s}2\pi}\int_0^{n_{f,s}2\pi}d\phi_{f,s0}\int_{-\infty}^{\infty}d\bar{u}_{\perp 0}\int_{-\infty}^{\infty}(\cdots)\times g(\bar{u}_{\perp 0},\bar{u}_{\parallel 0})d\bar{u}_{\parallel 0}=\frac{1}{n_{f,s}2\pi}\int_0^{n_{f,s}2\pi}d\phi_{f,s0}\int_{-\infty}^{\infty}(\cdots)h(\bar{p}_{f,s0})d\bar{p}_{f,s0}, \tag{11}$$

where subscript f,s is chosen as appropriate, $n_{f,s}$ is the integer number of fast/slow periods in a beat period ($\epsilon^3=n_f/n_s$) [4] and the functions $g(\bar{u}_\perp,\bar{u}_\parallel)$ and $h(\bar{p}_{f,s0})$ are normalized density distribution functions with the dependent variables being functions of the initial conditions $\phi_{f,s0}$ and $(\bar{u}_{\perp 0},\bar{u}_{\parallel 0})$ or $\bar{p}_{f,s0}$. In general, the relationship between the normalized density distribution functions $g(\bar{u}_{\perp 0},\bar{u}_{\parallel 0})$ and $h(\bar{p}_{f,s0})$ is not obvious, as the mapping $(\bar{u}_\perp,\bar{u}_\parallel)\rightarrow\bar{p}_{f,s}$ for each electron is obtained from the definition of $\bar{p}_{f,s}$ and may be expressed as a function of the scaling parameters as given in the Appendix.

III. LINEAR THEORY

We begin with a linear analysis of the coupled system of Eqs. (3)–(10). This is performed for the case of a finite spread in the scaled momentum of the electrons.

For convenience we make the following change of variables:

$$A_f'=\bar{A}_f e^{i\delta_f\bar{z}_f}\quad \phi_f'=\phi_f-\delta_f\bar{z}_f\quad p_f'=\bar{p}_f-\delta_f,$$

$$A_s'=\bar{A}_s e^{i\epsilon\delta_s\bar{z}_f}\quad \phi_s'=\phi_s-\epsilon\delta_s\bar{z}_f\quad p_s'=\bar{p}_s-\delta_s,$$

where $\delta_{f,s}=\langle\bar{p}_{f,s0}\rangle$ is the mean detuning of the electron beam from the resonance.

In order to describe a spread in the electron momentum about the initial mean of the beam, $\langle\bar{u}_{\parallel,\perp 0}\rangle=1$, a distribution parameter $(\Delta\bar{u}_{\parallel,\perp 0})$ is introduced, which is assumed small relative to the mean. In this way the initial electron momentum spread may be modeled using

$$\bar{u}_{\parallel,\perp 0_j}=1+\Delta\bar{u}_{\parallel,\perp 0_j} \tag{12}$$

for some symmetric distribution about zero of $\Delta\bar{u}_{\parallel,\perp 0_j}$, $(\Delta\bar{u}_{\parallel,\perp 0_j}\ll 1)$ over the electron index j.

Assuming subscript j where appropriate, the equilibrium values of the dependent variables are

$$A_{f,s0}'=0\quad \langle e^{-i\phi_{f,s0}'}\rangle=0\quad p_{f,s0}'=\bar{p}_{f,s0}-\delta_{f,s}\qquad \bar{u}_{\parallel,\perp 0}=1+\Delta\bar{u}_{\parallel,\perp 0}$$

corresponding to a uniformly distributed, unbunched beam, including momentum spread, with no initial field excitation at the beginning of the interaction region $\bar{z}_f=0$.

Linearizing around these equilibrium values the dependent variables are

$$A_{f,s}'=A_{f,s1}',$$

$$\phi_f'=\phi_{f0}'+\phi_{f1}'+p_{f0}'\bar{z}_f,$$

$$\phi_s'=\phi_{s0}'+\phi_{s1}'+\epsilon p_{s0}'\bar{z}_f,$$

$$p_{f,s}'=p_{f,s0}'+p_{f,s1}',$$

$$\bar{u}_{\parallel,\perp}=1+\Delta\bar{u}_{\parallel,\perp 0}+\bar{u}_{\parallel,\perp 1},$$

where all subscripts "1" denote small perturbations from the equilibrium values subscripted "0" at $\bar{z}_f=0$. Substituting for these variables into Eqs. (3)–(10) we obtain, to first order

$$\frac{d\phi_{f1}'}{d\bar{z}_f}=p_{f1}'-i(\mu_f A_{f1}'e^{i\phi_{f0}'}e^{ip_{f0}'\bar{z}_f}+\epsilon\mu_s A_{s1}'e^{i\phi_{s0}'}e^{i\epsilon p_{s0}'\bar{z}_f}-\text{c.c.}), \tag{13}$$

$$\frac{d\phi_{s1}'}{d\bar{z}_f}=\epsilon p_{s1}'-i(\mu_f A_{f1}'e^{i\phi_{f0}'}e^{ip_{f0}'\bar{z}_f}+\epsilon\mu_s A_{s1}'e^{i\phi_{s0}'}e^{i\epsilon p_{s0}'\bar{z}_f}-\text{c.c.}), \tag{14}$$

$$\frac{dp_{f1}'}{d\bar{z}_f}=((\rho_f[p_{f0}'+\delta_f]-1)A_{f1}'e^{i\phi_{f0}'}e^{ip_{f0}'\bar{z}_f}+(\epsilon\rho_s[p_{f0}'+\delta_f]-\epsilon^2\Omega)A_{s1}'e^{i\phi_{s0}'}e^{i\epsilon p_{s0}'\bar{z}_f}+\text{c.c.}), \tag{15}$$

$$\frac{dp'_{s1}}{d\bar{z}_f}=\left(\left(\rho_f[p'_{s0}+\delta_s]-\frac{\Omega}{\epsilon}\right)A'_{f1}e^{i\phi'_{f0}}e^{ip'_{f0}\bar{z}_f}+(\epsilon\rho_s[p'_{s0}+\delta_s]-\epsilon)A'_{s1}e^{i\phi'_{s0}}e^{i\epsilon p'_{s0}\bar{z}_f}+\text{c.c.}\right), \tag{16}$$

$$\frac{d\bar{u}_{\perp 1}}{d\bar{z}_f}=-(\mu_f A'_{f1}e^{i\phi'_{f0}}e^{ip'_{f0}\bar{z}_f}+\epsilon\mu_s A'_{s1}e^{i\phi'_{s0}}e^{i\epsilon p'_{s0}\bar{z}_f}+\text{c.c.}), \tag{17}$$

$$\frac{d\bar{u}_{\parallel 1}}{d\bar{z}_f}=-(\rho_f A'_{f1}e^{i\phi'_{f0}}e^{ip'_{f0}\bar{z}_f}+\epsilon\rho_s A'_{s1}e^{i\phi'_{s0}}e^{i\epsilon p'_{s0}\bar{z}_f}+\text{c.c.}), \tag{18}$$

$$\frac{dA'_{f1}}{d\bar{z}_f}=-i\langle\phi'_{f1}e^{-i\phi'_{f0}}e^{-ip'_{f0}\bar{z}_f}\rangle+\langle\bar{u}_{\perp 1}e^{-i\phi'_{f0}}e^{-ip'_{f0}\bar{z}_f}\rangle-\langle\bar{u}_{\parallel 1}e^{-i\phi'_{f0}}e^{-ip'_{f0}\bar{z}_f}\rangle+i\delta_f A'_{f1}, \tag{19}$$

$$\frac{dA'_{s1}}{d\bar{z}_f}=-i\epsilon\langle\phi'_{s1}e^{-i\phi'_{s0}}e^{-i\epsilon p'_{s0}\bar{z}_f}\rangle+\epsilon\langle\bar{u}_{\perp 1}e^{-i\phi'_{s0}}e^{-i\epsilon p'_{s0}\bar{z}_f}\rangle-\epsilon\langle\bar{u}_{\parallel 1}e^{-i\phi'_{s0}}e^{-i\epsilon p'_{s0}\bar{z}_f}\rangle+i\epsilon\delta_s A'_{s1}. \tag{20}$$

Note that for the purposes of linearization the terms $\Delta\bar{u}_{\parallel,\perp 0}$ are treated as first order as it has previously been assumed that all spreads are small, i.e., $\Delta\bar{u}_{\parallel,\perp 0}\ll 1$.

The linearized system, Eqs. (13)–(20), may be solved using the method of Laplace transforms, the complex Laplace transform being defined as

$$\tilde{X}(\lambda)=\int_0^\infty X(\bar{z}_f)e^{-i\lambda\bar{z}_f}d\bar{z}_f. \tag{21}$$

Applying the transform to the dependent variables, solving for the transformed field variables and inverting the transform we obtain a solution for the fields of

$$A'_{f,s}(\bar{z}_f)=\sum_{n=1}^{3}C_n\exp(i\lambda_{f,s_n}\bar{z}_f), \tag{22}$$

where C_n is a complex constant and the λ_{f,s_n} are the roots of the dispersion relations

$$\lambda_f-\delta_f+(\rho_f-2\mu_f)\int_{-\infty}^{+\infty}\frac{h(p'_{f0})}{(\lambda_f+p'_{f0})}dp'_{f0}+\int_{-\infty}^{+\infty}\frac{(1-\rho_f(p'_{f0}+\delta_f))h(p'_{f0})}{(\lambda_f+p'_{f0})^2}dp'_{f0}=0 \tag{23}$$

and

$$\lambda_s-\epsilon\delta_s+\epsilon^2(\rho_s-2\mu_s)\int_{-\infty}^{+\infty}\frac{h(p'_{s0})}{(\lambda_s+\epsilon p'_{s0})}dp'_{s0}+\epsilon^3\int_{-\infty}^{+\infty}\frac{(1-\rho_s(p'_{s0}+\delta_s))h(p'_{s0})}{(\lambda_s+\epsilon p'_{s0})^2}dp'_{s0}=0. \tag{24}$$

For convenience, the continuous limit average of Eq. (11) has been used where the initial spread in electron momentum gives a normalized density distribution of $h(p'_{f,s0})$. From Eq. (22), exponential growth of the fields can then be expected if the $\lambda_{f,s}$ from the solutions of Eqs. (23) and (24) have a negative imaginary part. As expected, the fast and slow modes are uncoupled in the linear regime of radiation evolution, each dispersion relation being independent of the other mode.

For an electron beam with no momentum spread the distribution function $h(p'_{f,s0})$ may be substituted by a Dirac-delta function $\delta(p'_{f,s0})$. The dispersion relations (23) and (24) then reduce to those derived previously for a cold electron beam [4].

The dispersion relations are now investigated for the specific case of uniform rectangular distributions in $p'_{f,s}$ of half width $\sigma_{f,s}$

$$h(p'_{f,s0})=\begin{cases}\dfrac{1}{2\sigma_{f,s}} & -\sigma_{f,s}\leqslant p'_{f,s0}\leqslant\sigma_{f,s}\\ 0 & \text{elsewhere.}\end{cases} \tag{25}$$

With these distributions, the fast and slow mode dispersion relations (23) and (24) reduce to the logarithmic forms

$$(\lambda_f-\delta_f)(\lambda_f^2-\sigma_f^2)+\rho_f\lambda_f-\frac{\mu_f(\lambda_f^2-\sigma_f^2)}{\sigma_f}\ln\left(\frac{\lambda_f+\sigma_f}{\lambda_f-\sigma_f}\right)+(1-\rho_f\delta_f)=0, \tag{26}$$

$$(\lambda_s-\epsilon\delta_s)(\lambda_s^2-\epsilon^2\sigma_s^2)+\epsilon^2\rho_s\lambda_s-\frac{\epsilon\mu_s(\lambda_s^2-\epsilon^2\sigma_s^2)}{\sigma_s}\ln\left(\frac{\lambda_s+\epsilon\sigma_s}{\lambda_s-\epsilon\sigma_s}\right)+\epsilon^3(1-\rho_s\delta_s)=0. \tag{27}$$

Where there is no spread ($\sigma_{f,s}\to 0$) then, as required, the dispersion relations reduce to those previously derived for a cold electron beam [3,4].

In the low efficiency limit of $\rho_{f,s},\mu_{f,s}\to 0$ the following dispersion relations are obtained:

$$(\lambda_f-\delta_f)(\lambda_f^2-\sigma_f^2)+1=0, \tag{28}$$

$$(\lambda_s-\epsilon\delta_s)(\lambda_s^2-\epsilon^2\sigma_s^2)+\epsilon^3=0. \tag{29}$$

These dispersion relations are identical in form to those obtained for the Compton free electron laser when momentum spread effects in the electron beam are taken into account, e.g., Ref. [7]. In the limit $\delta_{f,s}\to 0$ there is a threshold in the

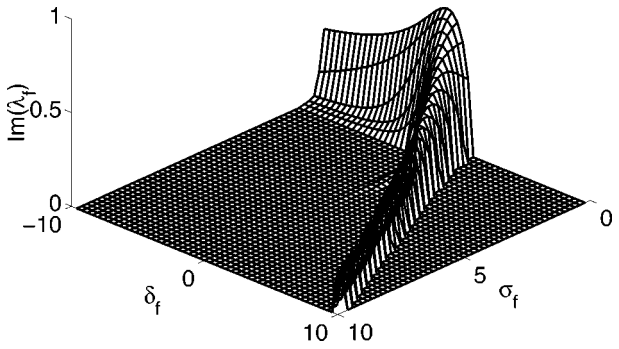

FIG. 3. Gain curve for the fast mode $\rho_f=0.0681$, $\mu_f=0.252$.

spread of $p'_{f,s}$, at $\sigma_{f,s}=(27/4)^{1/6}$, above which no complex roots exist and there can be no exponential growth of the fields. Furthermore, it can be shown that maximum gain occurs when the detuning is equal to the spread, $\delta_{f,s}=\sigma_{f,s}$.

In Fig. 3 the negative imaginary part of the complex root obtained from a solution of the full dispersion relation (26), which determines the exponential gain for the fast mode, is plotted as a function of electron beam detuning δ_f and spread σ_f, for given values of ρ_f and μ_f. Numerical solutions of the logarithmic dispersion relations were obtained by using the mathematical computer package MAPLE [8]. As with the low efficiency limit of above, it can be seen that maximum gain occurs for an electron detuning parameter of $\delta_f\approx\sigma_f$. A similar plot is obtained for the slow mode and, similarly, maximum growth is obtained for $\delta_s\approx\sigma_s$.

A comparison of the growth rates of the competing fast and slow modes in the presence of electron beam momentum spread is now presented. Of particular interest is the effect of such a spread in the μ-suppression regime where, for zero momentum spread, the fast mode has a larger growth rate than the slow mode. It is assumed that the density distribution of electrons in momentum space, $g(\overline{u_\perp},\overline{u_\parallel})$, results in a rectangular distribution $h(\overline{p'_{f,s}})$ in p' space of the form (25). The relationship between σ_f and σ_s is obtained from the analysis of Appendix A. As suggested by the above analysis and the results of Fig. 3, a detuning $\delta_{f,s}=\sigma_{f,s}$ is chosen in an attempt to maximize the gain for both modes. The values for $\delta_{f,s}$ which actually maximize these gains may be slightly different, however the results presented are not significantly affected.

The difference between the fast and slow negative imaginary parts of the complex roots, $\mathrm{Im}(\lambda_f-\lambda_s)$, obtained from a solution of the full dispersion relations (26) and (27), is plotted as a function of μ_f for four values of electron momentum spread and is shown in Fig. 4 . For negative values of the difference, the slow mode has the larger growth rate and would dominate any interaction for equal input fields. For positive values the higher frequency fast mode will dominate. This has previously been called the μ-suppression regime [4]. For the case of no electron momentum spread ($\sigma_f=0$), it is seen that on increasing μ_f from zero, suppression of the slow mode begins to take effect at $\mu_f\approx0.5$. On increasing μ_f further, both roots are nonzero until μ_f ($=\mu_{th}$)≈0.68 after which there are no complex roots for the slow mode ($\lambda_s=0$) and the value plotted is entirely due to

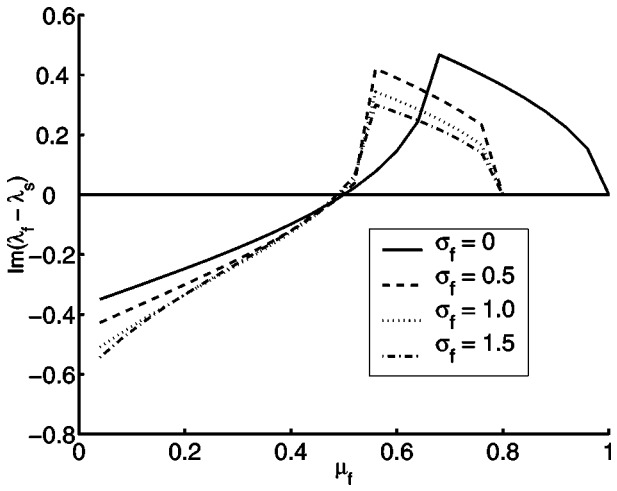

FIG. 4. $\mathrm{Im}(\lambda_f-\lambda_s)$ against μ_f for the fast and slow mode. When $\mathrm{Im}(\lambda_f-\lambda_s)>0$ the system is in the μ suppression regime where the fast mode growth rate is greater than the slow mode: $\rho_f=0.1$; $\epsilon^3=3$; $\delta_{f,s}=\sigma_{f,s}$.

the fast root λ_f. For values of $\mu_f\gtrsim1.0$, $\lambda_f=0$ and there can be no exponential growth of either the slow or the fast mode. For $\sigma_f=0$ then, μ suppression of the slow mode occurs between the limits $0.5<\mu_f<0.97$. Note that this range of μ_f for μ suppression is extended below the minimum of that predicted in Ref. [4]. This is because μ suppression was defined to start at the threshold value for *zero* growth of the slow mode. This value here is ≈0.68. In the region $0.5\leqslant\mu_f\leqslant0.68$ of Fig. 4 slow mode growth exists but is less than that of the fast mode.

When the effects of electron momentum spread are included, $\sigma_f=0.5,1.0,1.5$ (and we allow optimum detuning, $\delta_{f,s}=\sigma_{f,s}$) we observe that, as would be expected from the discussion above, the growth rates of the fields are reduced, as is the range over which μ suppression of the slow mode is possible, quickly reducing the interval to $0.5\lesssim\mu_f\lesssim0.8$. The results shown in Fig. 4 are in good agreement with growth rates calculated via numerical integration of Eqs. (3)–(10).

IV. COMPARISON WITH NUMERICAL MODEL

The growth rates predicted from the solutions to the dispersion relations (26) and (27) are now compared with those obtained from a full numerical solution to Eqs. (3)–(10). In carrying out this comparison, it was found necessary to artificially ''switch off'' the evolution of one of the modes in the full numerical solution as a mode coupling is quickly established and the interaction departs from that of linear theory well before saturation of the fast mode. With such artificial mode decoupling it is found there is a good agreement between the numerical and linear models in determining the growth rates over a wide range of parameter space.

An example of this agreement is shown in Fig. 5 where the growth rates for the fast mode are plotted as functions of spread σ_f. Plot (a) shows the analytical solution of the linear theory and plots (b) and (c) show two numerical solutions. The first numerical solution [Fig. 5(b)] assumes a uniform

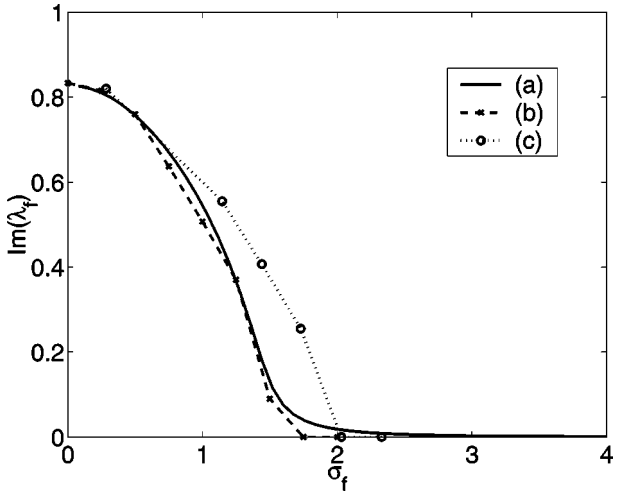

FIG. 5. A comparison between growth rates as calculated via the linear theory and numerical integration for $\rho_f=0.0681, \mu_f=0.1, \delta_{f,s}=0, \epsilon^3=3$. (a) Linear theory, (b) rectangular distribution over $\bar{p}_f$ of width σ_f, (c) rectangular distribution over $\bar{u}_{\perp,\parallel}$ of widths $\sigma_\perp=\sigma_\parallel$.

rectangular distribution in $\bar{p}_f$ of half width σ_f of the form (25) and it is seen that the growth rates of this numerical model agree very well with that of linear theory. The second numerical solution [Fig. 5(c)] is for a uniform rectangular distribution in both $\bar{u}_\perp$ and $\bar{u}_\parallel$ of equal width $\sigma_\perp=\sigma_\parallel$. These spreads in $(\sigma_\perp,\sigma_\parallel)$ correspond to a spread in σ_f via the relation (A9) of Appendix A. A rectangular distribution function in $(\bar{u}_\perp,\bar{u}_\parallel)$ does not, however, map into the uniform rectangular distribution in $\bar{p}_f$ as used in the linear theory. The difference between Figs. 5(a) and 5(c) is attributed to this.

V. EXPERIMENTAL PARAMETERS

The work presented above attempts to model more realistically two frequency CRM amplifier experiments under development at the University of Strathclyde. Using these results it is hoped to find regions of parameter space where it is possible to observe the predicted higher frequency CRM operation. In this section we give numerical solutions to the scaled Eqs. (3)–(10) demonstrating the effects of momentum spread on the two frequency interaction of the experiments. The equations are solved with initial conditions corresponding to an amplifier configuration, with initial fields given by $\bar{A}_{f,s}(\bar{z}_f=0)=\bar{A}_{f,s0}$, where $\bar{A}_{f,s0}$ are constants; the electrons are initially distributed evenly in phase with zero bunching so that $\langle\exp(-i\phi_{f,s0})\rangle=0$ [4]; and the electron momentum spread distribution function $g(\bar{u}_\perp,\bar{u}_\parallel)$, of Eq. (11), is now assumed to be a Gaussian in both $\bar{u}_\perp$ and $\bar{u}_\parallel$ with corresponding widths $\sigma_{\perp,\parallel}$. The real input–output radiation power is calculated via the complex Poynting vector [9], the definition of the fields and the scaling used in Eqs. (3) - (10).

The experimental parameters are given below in Table I along with the corresponding scaled parameters.

Figure 6 shows the effect of momentum spread on the resonant ($\delta_{f,s}=0$) operation of the two frequency CRM in the μ suppression regime. The momentum spreads were calculated numerically from electron beam modeling work of the thermionic cathode to be used in the experiment. This work predicts that the momentum spread may be attributed mainly to the velocity spread of the beam of which the axial velocity spread is estimated to be not more than $\approx 1\%$ [10]. The experimental interaction was modeled for different values of spread for the transverse component of the electron momentum and it is seen that μ suppression of the slow mode persists. For larger transverse momentum spreads the growth rate of the fast mode interaction is reduced and a longer interaction region is required to reach saturation. However, if the spread in the axial momentum component is increased from 1% to 2–3%, it has been observed that the fast mode intensity is sharply reduced. This result, and the expression for the scaled momentum spread in Eq. (A9), suggests that the sensitivity of the system to axial momentum spread increases as the device parameter, Ω, tends towards

TABLE I. Proposed experimental parameters for the slow mode suppression and stimulated emission experiments.

	μ suppression	Stimulated emission
Magnetic guiding field	0.28 T	0.29 T
Electron beam current	39.5 A	36 A
Electron beam energy	367 keV	466 keV
Relativistic Lorentz factor (γ)	1.72	1.91
Beam pitch factor (α)	0.15	0.30
Fast mode frequency	17.3 GHz	17.0 GHz
Slow mode frequency	8.0 GHz	8.5 GHz
TE_{11} cutoff frequency	6.72 GHz	6.72 GHz
Wave number ratio (ϵ^3)	3.6	3.0
Device parameter (Ω)	1.52	1.4
Fundamental CRM parameter (ρ_f)	0.048	0.068
Free energy depletion (μ_f)	0.71	0.252

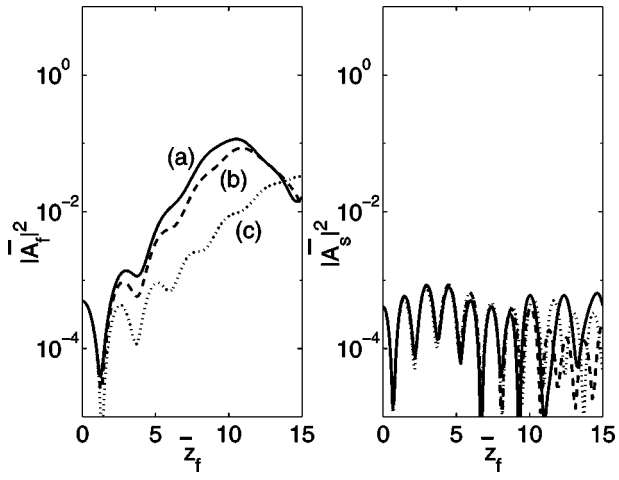

FIG. 6. Two mode evolution in the μ-suppression regime with electron beam momentum spread (a) $\sigma_{\parallel,\perp}=0$, (b) $\sigma_\parallel=1\%$, $\sigma_\perp=10\%$, (c) $\sigma_\parallel=1\%$, $\sigma_\perp=20\%$, $\rho_f=0.048, \mu_f=0.71, \epsilon^3=3.6, \Omega=1.52$: $\bar{A}_{fo}=0.0222(\approx 400\ \mathrm{W})$, $\bar{A}_{so}=0.0203(\approx 400\ \mathrm{W})$.

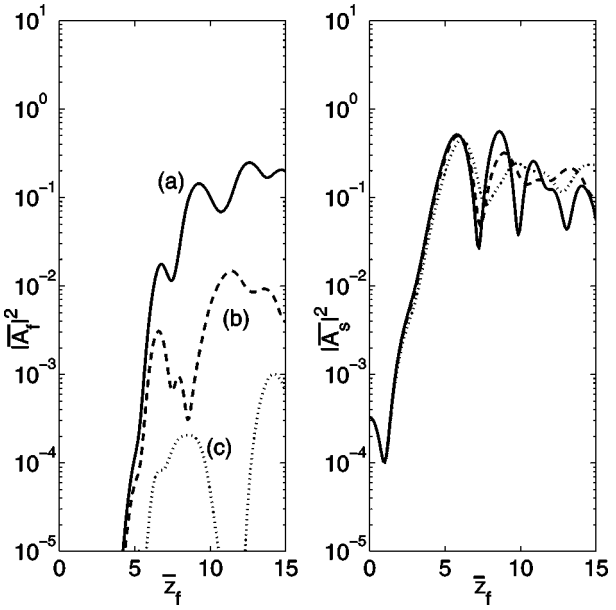

FIG. 7. Stimulated emission at the high frequency interaction point for various momentum spreads: (a) $\sigma_{\|,\perp}=0$, (b) $\sigma_{\|}=0.5\%$, $\sigma_{\perp}=5\%$, (c) $\sigma_{\|}=1\%$, $\sigma_{\perp}=10\%$: input power ≈ 400 W ($|\overline{A}_{s0}|^2=3.29\times10^{-4}$). Fast mode output (a) $|\overline{A}_f|^2_{max}\approx 0.23$($\approx 250$ kW), (b) $|\overline{A}_f|^2_{max}\approx 0.01$ (≈ 12 kW), (c) $|\overline{A}_f|^2_{max}\approx 0.001$ (≈ 1 kW).

the CARM limit, ($\Omega\rightarrow\Omega_{max}$). This is in agreement with other CARM studies where performance is known to depend on the axial momentum spread when operating in the CARM regime, e.g., Ref. [11].

Stimulated emission of radiation at the high fast mode frequency, given only an injected signal at the lower slow mode frequency [4], was studied with an electron beam momentum spread into the nonlinear regime. This stimulated emission is greatest for a harmonic interaction, i.e., when ϵ^3 is an integer.

A cold beam interacting with input intensities $|\overline{A}_{s0}|^2\approx 3.29\times10^{-4}$ (≈ 400 W) and $|\overline{A}_{f0}|^2=0$ is shown in Fig. 7(a). The lower frequency saturates at $|\overline{A}_s|^2\approx 0.52$ (≈ 600 kW) and the higher frequency has a maximum of $|\overline{A}_f|^2\approx 0.23$ (≈ 250 kW).

When momentum spread is introduced the output intensities are seen to reduce as expected from Figs. 7(b) and 7(c). The maximum intensities [for a momentum spread of $\sigma_{\perp}=10\%$ and $\sigma_{\|}=1\%$ Fig. 7(c)] are $|\overline{A}_s|^2=0.46(\approx 500$ kW) and $|\overline{A}_f|^2=0.001(\approx 1$ kW). It should be noted that by increasing the input intensity at the lower frequency to $\gtrsim 4$ kW, output at the higher frequency may be increased to $\gtrsim 10$ kW.

VI. CONCLUSIONS

An analysis of the cyclotron resonance maser (CRM) operating at two resonant frequencies and including the effects of electron momentum spread has been presented. The linear analysis yielded a logarithmic dispersion relation to give the linear growth rates for both resonant frequencies. These were found to be in good agreement with those calculated via a numerical integration of the system equations. The numerical simulations have allowed a study of the nonlinear behavior of the CRM, in particular the effect of momentum spread on the μ suppression and ''stimulated emission'' regimes of operation for forthcoming experiments. The simulations predict that, with modest beam quality, it should be possible to generate significant output at the higher resonant frequency in both regimes of operation.

ACKNOWLEDGMENTS

The authors would like to thank the EPSRC for support of G.J.H. and B.W.J.McN., and the Royal Society of Edinburgh for support of G.R.M.R. The authors' thanks are also extended to A. R. Young for providing numerical estimates of expected experimental electron beam quality.

APPENDIX

By expressing the physical parameters of the system in terms of the scaled parameters

$$k_f=\frac{\omega_c\epsilon^3}{c}\sqrt{\left(\frac{(\Omega^2-1)}{\epsilon^6-2\Omega\epsilon^3+1}\right)},\quad k_s=\frac{k_f}{\epsilon^3},\tag{A1}$$

$$\omega_f=\omega_c\frac{(\epsilon^3\Omega-1)}{\sqrt{(\epsilon^6-2\Omega\epsilon^3+1)}},\quad \omega_s=\omega_c\frac{(\epsilon^3-\Omega)}{\sqrt{(\epsilon^6-2\Omega\epsilon^3+1)}},\tag{A2}$$

$$\langle\beta_{\|0}\rangle=\frac{(\epsilon^2-\epsilon+1)(\epsilon+1)}{(\epsilon^2+\epsilon+1)(\epsilon-1)}\sqrt{\left(\frac{\Omega-1}{\Omega+1}\right)},\tag{A3}$$

$$\omega_H=\omega_c\frac{\sqrt{(\epsilon^6-2\epsilon^3\Omega+1)}}{(\epsilon^2+\epsilon+1)(\epsilon-1)},\tag{A4}$$

$$\langle\gamma_0\rangle=(\epsilon^2+\epsilon+1)(\epsilon-1)\times\sqrt{\frac{\mu_f\epsilon^3(\Omega+1)}{(\epsilon^6-2\epsilon^3\Omega+1)(2\mu_f\epsilon^3-\rho_f(\epsilon^3+1))}}\tag{A5}$$

and by using the definition of $\overline{p_{f,s}}$, it is possible to obtain the functional relation $\overline{p}_{f,s}(\overline{u}_{\perp},\overline{u}_{\|})$

$$\overline{p}_f=\frac{\gamma}{\overline{u}_{\|}}\frac{\epsilon^2(\epsilon^3\Omega-1)}{\rho_f(\epsilon^3+1)}\sqrt{\frac{(2\mu_f\epsilon^3-\rho_f(\epsilon^3+1))(\Omega+1)}{\mu_f(\epsilon^6-2\Omega\epsilon^3+1)}}-\frac{1}{\overline{u}_{\|}}\frac{\epsilon^3(\Omega+1)}{\rho_f(\epsilon^3+1)}-\frac{\epsilon^6(\Omega^2-1)}{\rho_f(\epsilon^6-2\Omega\epsilon^3+1)},\tag{A6}$$

$$\overline{p}_s=\frac{\gamma}{u_\parallel}\frac{(\epsilon^3-\Omega)}{\rho_f(\epsilon^3+1)}\sqrt{\frac{\epsilon(2\mu_f\epsilon^3-\rho_f(\epsilon^3+1))(\Omega+1)}{\mu_f(\epsilon^6-2\Omega\epsilon^3+1)}}-\frac{1}{u_\parallel}\frac{\epsilon^2(\Omega+1)}{\rho_f(\epsilon^3+1)}-\frac{\epsilon^2(\Omega^2-1)}{\rho_f(\epsilon^6-2\Omega\epsilon^3+1)}, \tag{A7}$$

where

$$\gamma=\sqrt{1+\overline{u}_\perp^2\frac{\rho_f(\epsilon^3+1)}{2\mu_f\epsilon^3-\rho_f(\epsilon^3+1)}+\overline{u}_\parallel^2\frac{\mu_f\epsilon^3(\epsilon^3+1)^2(\Omega-1)}{(\epsilon^6-2\Omega\epsilon^3+1)(2\mu_f\epsilon^3-\rho_f(\epsilon^3+1))}}. \tag{A8}$$

An estimate of the spread in $\overline{p}_{f,s}$ can then be made by assuming the small spreads in $\overline{u}_{\parallel,\perp}$. Assuming the maximum range of values is given by $\overline{u}_{\parallel,\perp}^{(max)}\approx 1+\sigma_{\parallel,\perp}$, where $\sigma_{\parallel,\perp}\ll 1$ and are positive definite, then we may substitute for $\overline{u}_{\parallel,\perp}^{(max)}$ into Eqs. (A6) and (A7) and expand to first order in $\sigma_{\parallel,\perp}$. Thus, an estimate of the spread in $\overline{p}_{f,s}$, defined as $\sigma_{f,s}$ is given by

$$\sigma_f\approx\frac{\Omega\epsilon^3-1}{\mu_f(\epsilon^3-1)}\sigma_\perp+\frac{\epsilon^3(\Omega-1)}{\rho_f(\epsilon^3-1)}\sigma_\parallel, \tag{A9}$$

$$\sigma_s\approx\frac{(\epsilon^3-\Omega)}{\epsilon\mu_f(\epsilon^3-1)}\sigma_\perp+\frac{\epsilon^2(\Omega-1)}{\rho_f(\epsilon^3-1)}\sigma_\parallel. \tag{A10}$$

[1] *High-Power Microwave Sources*, edited by V. L. Granatstein and I. Alexeff (Artech, Boston, 1987).

[2] P. Sprangle and A. T. Drobot, IEEE Trans. Microwave Theory Tech. **25**, 528 (1977).

[3] B. W. J. McNeil, G. R. M. Robb, and A. D. R. Phelps, J. Phys. D **27**, 1092 (1994).

[4] P. Aitken, B. W. J. McNeil, G. R. M. Robb, and A. D. R. Phelps, J. Phys. D **30**, 2482 (1997).

[5] P. Aitken, B. W. J. McNeil, G. R. M. Robb, and A. D. R. Phelps, Phys. Rev. E **59**, 1152 (1999).

[6] J. R. Pierce, *Travelling—Wave Tubes* (Van Nostrand, New York, 1950).

[7] R. Bonifacio, F. Casagrande, G. Cerchioni, L. De Salvo Souza, P. Pierini, and N. Piovella, Riv. Nuovo Cimento **9** (1990).

[8] Maple V, version 5, Waterloo Maple Inc. (1997).

[9] J. D. Jackson, *Classical Electrodynamics* (Wiley, New York, 1975).

[10] A. R. Young (private communication).

[11] A. C. DiRienzo, G. Bekefi, C. Chen, and J. S. Wurtele, Phys. Fluids B **3**, 1755 (1991).